

Photonic crystal-based all-optical on-chip sensor

Y. Liu^{1,2} and H. W. M. Salemink^{1,*}

¹Department Kavli Institute of Nanoscience, Lorentzweg 1, 2628 CJ Delft, The Netherlands

²Foundation for Fundamental Research on Matter, Van Vollenhovenlaan 659, 3527 JP, Utrecht, The Netherlands

*H.W.M.Salemink@tudelft.nl

Abstract: In this paper we demonstrate a sensor based on a two-dimensional photonic crystal cavity structure. Design, theoretical simulations, fabrication and experiments are shown to illustrate the working principle of this device. Sensitivity of our sensor is determined by observing the shift of resonant wavelength of the photonic crystal cavity as a function of the refractive index variation of the analyte. By experimentally infiltrating solutions of water and ethanol through an elastomeric micro-fluidic channel, we have confirmed that our all-optical sensor achieves a sensitivity of 460 nm/RIU.

©2012 Optical Society of America

OCIS codes: (050.5298) Photonic crystals; (130.6010) Sensors; (230.7400) Waveguides, slab.

References and links

1. O. Levi, M. Lee, J. Zhang, V. Lousse, S. Brueck, S. Fan, and J. Harris, "Sensitivity analysis of a photonic crystal structure for index-of-refraction sensing," Proc. SPIE **6447**, 64470P (2007).
2. M. Adams, G. DeRose, M. Loncar, and A. Scherer, "Lithographically fabricated optical cavities for refractive index sensing," J. Vac. Sci. Technol. B **23**(6), 3168–3173 (2005).
3. J. Homola, S. Yee, and G. Gauglitz, "Surface plasmon resonance sensors: review," Sens. Actuators B Chem. **54**(1-2), 3–15 (1999).
4. A. Ymeti, J. S. Kanger, J. Greve, G. A. Besselink, P. V. Lambeck, R. Wijn, and R. G. Heideman, "Integration of microfluidics with a four-channel integrated optical Young interferometer immunosensor," Biosens. Bioelectron. **20**(7), 1417–1421 (2005).
5. R. Kunz, "Miniature integrated optical modules for chemical and biochemical sensing," Sens. Actuators B Chem. **38**(1-3), 13–28 (1997).
6. E. Udd and W. Spillman, *Fiber Optic Sensors—an Introduction for Engineers and Scientists* (Wiley, 2011).
7. J. Jensen, P. Hoiby, G. Emiliyanov, O. Bang, L. Pedersen, and A. Bjarklev, "Selective detection of antibodies in microstructured polymer optical fibers," Opt. Express **13**(15), 5883–5889 (2005).
8. L. Rindorf, J. B. Jensen, M. Dufva, L. H. Pedersen, P. E. Høiby, and O. Bang, "Photonic crystal fiber long-period gratings for biochemical sensing," Opt. Express **14**(18), 8224–8231 (2006).
9. R. W. Boyd and J. E. Heebner, "Sensitive disk resonator photonic biosensor," Appl. Opt. **40**(31), 5742–5747 (2001).
10. Y. Akahane, T. Asano, B. S. Song, and S. Noda, "High-Q photonic nanocavity in a two-dimensional photonic crystal," Nature **425**(6961), 944–947 (2003).
11. Y. Akahane, T. Asano, B. S. Song, and S. Noda, "Fine-tuned high-Q photonic-crystal nanocavity," Opt. Express **13**(4), 1202–1214 (2005).
12. B. Song, S. Noda, T. Asano, and Y. Akahane, "Ultra-high-Q photonic double-heterostructure nanocavity," Nat. Mater. **4**(3), 207–210 (2005).
13. T. Asano, B. S. Song, and S. Noda, "Analysis of the experimental Q factors (~ 1 million) of photonic crystal nanocavities," Opt. Express **14**(5), 1996–2002 (2006).
14. S. Johnson, S. Fan, P. Villeneuve, J. Joannopoulos, and L. Kolodziejski, "Guided modes in photonic crystal slabs," Phys. Rev. B **60**(8), 5751–5758 (1999).
15. T. Krauss and R. De La Rue, "Photonic crystal in the optical regime-past, present and future," Prog. Quantum Electron. **23**(2), 51–96 (1999).
16. N. Mortensen, S. Xiao, and J. Pedersen, "Liquid-infiltrated photonic crystals: enhanced light-matter interactions for lab-on-a-chip applications," Microfluid. Nanofluid. **4**(1–2), 117–127 (2008).
17. F. Hsiao and C. Lee, "Nanophotonic biosensors using hexagonal nanoring resonators: computational study," J. Micro/Nanolithogr. MEMS MOEMS **10**(1), 013001 (2011).
18. C. Kang, C. T. Phare, Y. A. Vlasov, S. Assefa, and S. M. Weiss, "Photonic crystal slab sensor with enhanced surface area," Opt. Express **18**(26), 27930–27937 (2010).
19. X. Serey, S. Mandal, and D. Erickson, "Comparison of silicon photonic crystal resonator designs for optical trapping of nanomaterials," Nanotechnology **21**(30), 305202 (2010).

20. D. Dorfner, T. Zabel, T. Hürlmann, N. Hauke, L. Frandsen, U. Rant, G. Abstreiter, and J. Finley, "Photonic crystal nanostructures for optical biosensing applications," *Biosens. Bioelectron.* **24**(12), 3688–3692 (2009).
 21. E. Guillermain and P. Fauchet, "Multi-channel biodetection via resonant microcavities coupled to a photonic crystal waveguide," *Proc. SPIE* **7167**, 71670D (2009).
 22. S. C. Buswell, V. A. Wright, J. M. Burriak, V. Van, and S. Evoy, "Specific detection of proteins using photonic crystal waveguides," *Opt. Express* **16**(20), 15949–15957 (2008).
 23. S. Mandal, R. Akhmechet, L. Chen, S. Nugen, A. Baeumner, and D. Erickson, "Nanoscale optofluidic sensor arrays for dengue virus detection," *Proc. SPIE* **6645**, 66451J (2007).
 24. S. Mandal and D. Erickson, "Nanoscale optofluidic sensor arrays," *Opt. Express* **16**(3), 1623–1631 (2008).
 25. M. Lončar, A. Scherer, and Y. Qiu, "Photonic crystal laser sources for chemical detection," *Appl. Phys. Lett.* **82**(26), 4648–4650 (2003).
 26. M. L. Adams, M. Loncar, A. Scherer, and Y. Qiu, "Microfluidic integration of porous photonic crystal nanolasers for chemical sensing," *IEEE J. Sel. Areas Comm.* **23**(7), 1348–1354 (2005).
 27. T. Tanabe, M. Notomi, and E. Kuramochi, "Measurement of ultra-high-Q photonic crystal nanocavity using single-sideband frequency modulator," *Electron. Lett.* **43**(3), 187–188 (2007).
 28. A. Oskooi, D. Roundy, M. Ibanescu, P. Bermel, J. Joannopoulos, and S. Johnson, "MEEP: A flexible free-software package for electromagnetic simulations by the FDTD method," *Comput. Phys. Commun.* **181**(3), 687–702 (2010).
 29. J. Berenger, "A perfectly matched layer for the absorption of electromagnetic waves," *J. Comput. Phys.* **114**(2), 185–200 (1994).
 30. V. Mandelshtam and H. Taylor, "Harmonic inversion of time signals and its applications," *J. Chem. Phys.* **107**(17), 6756–6770 (1997).
 31. Y. Akahane, T. Asano, B. S. Song, and S. Noda, "High-Q photonic nanocavity in a two-dimensional photonic crystal," *Nature* **425**(6961), 944–947 (2003).
-

1. Introduction

Sensitive sensors are of crucial importance for both academia and industry in environmental monitoring and biological safety investigation. The working principle of these passive optical sensors relies on the variations of their optical properties when the refractive index (RI) of the analyte changes [1,2]. The most well exploited techniques for optical sensing are based on the principle of surface plasmon resonance (SPR) [3], interferometry [4], and optical resonance. Surface Plasmon resonance devices [5], optical waveguides/photonic crystal fibers (PCF) [6] which have been demonstrated for sensing antibodies [7] and DNA [8], as well as disk/ring resonators [9] are common examples of such applications.

Investigation on sensors relying on optical resonance is a hot research topic. Optical resonance leads to dips or peaks in the spectral signature. When the refractive indices are modified, wavelength-shifts of the dips or peaks are traceable. With precise calibration, the shifts may even work as the fingerprint identification.

Among those optical resonance sensors, photonic crystal sensors show advantages in integrated lab-on-a-chip systems with their small footprint and high quality factor/volume. Photonic crystals (PhC) are periodic structures with a defined lattice constant. The photonic bandgap arises from photon scattering in a similar way of the semiconductor electronic bandgap. Photons with frequencies inside the bandgap do not propagate through photonic crystal. However, new photonic energy states can be created by introducing "defects" in photonic crystal. These "defects" are identified as optical cavities with particular resonant dips/peaks in the spectral signature. Photons are confined in the cavity at resonant wavelengths. It has been proved, with fine structural optimization, a photonic crystal cavity can have a quality factor (Q) as high as 10^6 [10–13] in very small dimensions [14,15], on the order of λ^3 , which enhances the light-matter interaction and reduces the interaction volume. Therefore, tiny variations in refractive index are measureable and reflected in the optical properties of the photonic crystal cavities. A potential utilization of these features is to be used as an on-chip label-free biosensor in planar geometries [16]. PhC-based biosensors detect molecules attached to the surface (surface-based sensing) via monitoring of the deviation of optical characters [17–23]. In addition, photonic crystal cavities are fabricated with standard semiconductor techniques. A typical planar photonic crystal consists of cylindrical air holes with defined lattice constant in a thin silicon membrane. These devices

can be fabricated using microelectronic fabrication techniques, and can be easily integrated with microelectronics, microfluidics [23,24], and other kinds of photonic devices.

Photonic crystal sensors rely on the interaction between light and analyte. However, in some cases, optical modes are tightly confined at the center of cavities in both horizontal and vertical directions, leaving very small portions of evanescent light existing outside the cavity. Under such situations, interactions between the analyte and the evanescent light are too weak to induce a clear variation of the optical properties. Thus, a key challenge for photonic crystal sensors is the limited spatial overlap between light and analyte. Many researches are targeting at this problem, such as thinning the thickness of cavities or using a H_0 “defect” with an enlarged air hole instead of a solid-filled “defect” [25,26]. Nevertheless, those approaches reduce light confinement and decrease Q factors seriously. Therefore, tradeoffs between spatial overlap and light confinement are needed.

Here we present our investigation towards the development of a L7-cavity-based on-chip sensor that allows us to overcome the above limitations. As will be demonstrated, our sensor has more than one resonant wavelength within the bandgap at different transmission bands. These simultaneous resonances can be used for establishing the RI modification and avoiding false detection of wavelength shifts. More importantly, we enlarge the spatial overlap between the photonic crystal cavity and the analyte by directly introducing unique mini air holes inside the cavity with size and location optimization. Our theoretical analysis shows that the introduction of these additional mini air holes increases detection sensitivity without significantly decreasing the Q factor. Introducing air holes into the cavities enables a wavelength shift of 12.65nm under a small refractive index modification of 2.7E-2.

2. Design

Figure 1 shows a PhC microcavity in a silicon-on-insulator (SOI) wafer. The investigated structure consists of air holes being etched through the silicon membrane. Photonic crystal cavity is formed by solid-filling seven air holes in the Γ -K direction. The confinement of light in the vertical direction is ensured by total internal reflection (TIR) at the interfaces between the silicon membrane and lower refractive index materials both beneath and above the membrane. The structure shown here has the lattice constant a and the radius of the air holes r , $r/a = 0.33$. The thickness h of the silicon membrane equals to $h/a = 0.427$ and its refractive index $n_{\text{slab}} = 3.4$. In order to make the sensor work near the wavelength of 1550nm, we choose the parameters as follows: $a = 515\text{nm}$, $h = 220\text{nm}$, $r = 170\text{nm}$.

The Q factor of the cavity is firstly tuned by varying the geometric parameters of the air holes around the “defect”. According to those previous investigations on high Q cavity design, light confinement can be optimized by adjusting the profile of electromagnetic-field distribution of the resonant optical mode. Enhancing the confinement in perpendicular direction [27], smoothing the field distribution at the boundaries [11], and creating band edge

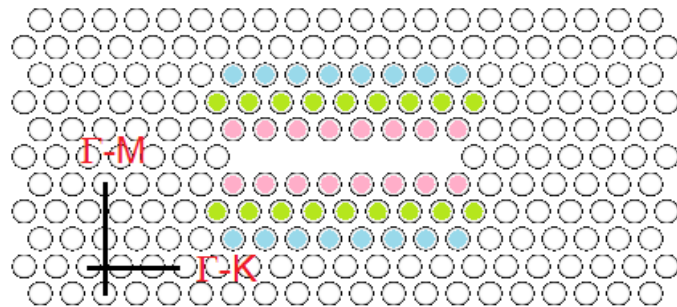


Fig. 1. The L7 cavity in photonic crystal with width modification. Three neighboring rows of air holes (filled with pink, green and blue colors) are shifted outwardly by $0.02a$, $0.014a$ and $0.007a$.

mismatching [13] are all efficient methods in achieving high Q cavities. Here we use those concepts to increase the Q factor of our sensor. The width of the cavity is modified by locally slightly shifting three neighboring rows of air holes away from the cavity center in the Γ -M direction, with shifting distances of $0.02a$, $0.014a$ and $0.007a$, which are 10.3nm, 7.2nm and 3.6nm for our sensor. These modifications result in an enhanced light confinement and provide a Q factor increase of ~ 1000 , compared to an unmodified L7 cavity.

A three-dimensional finite difference time domain (FDTD) simulation program of MEEP [28] is performed in order to examine the effect of adding mini air holes into the L7 cavity. All dimensions are normalized to the lattice constant a . At the first step of our design, the silicon slab is fully exposed to air of which refractive index is 1.0 in our simulation. The cavity is surrounded by 7 rows of air holes in the Γ -K direction, and 6 rows of air holes in the Γ -M direction. The entire simulation region is surrounded by a perfectly matched layer (PML) with a thickness of $2.0 a$, absorbing any residual light at boundaries [29]. The resonant frequencies and quality factors are computed by the software of harmonic inversion (the built-in “harminv” in MEEP) [30], which decouple the cavity fields into individual sinusoids and calculate their decay rates. A broadband pulse is placed inside the L7 cavity as a TE-polarized dipole point source with Gaussian frequency distribution to excite the cavity modes. The light source has offsets of $0.1 a$ in both Γ -K and Γ -M directions in order to excite all possible optical modes regardless of modes’ symmetry. Resonant modes maintain high Q factors after 400 time periods after the excitation.

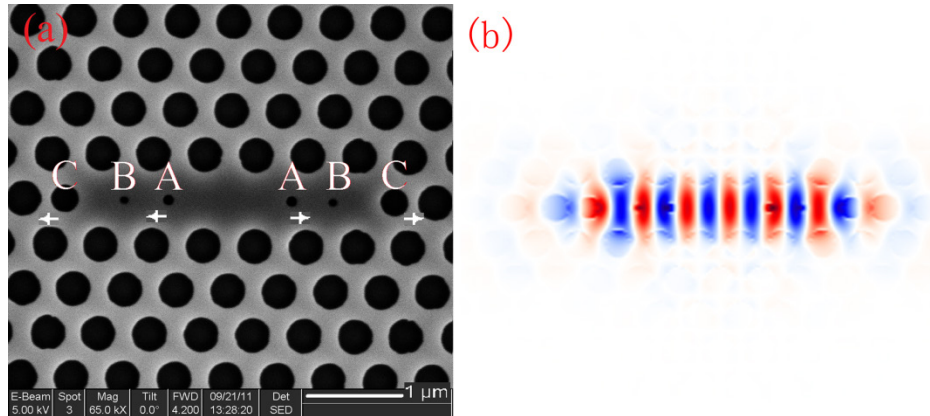


Fig. 2. (a) Scanning electron microscope image of the sensor device. $r_c = 132.6\text{nm}$, $d_c = 103\text{nm}$; $r_b = 34\text{nm}$, $d_b = 0$; $r_a = 47.6\text{nm}$, $d_a = 103\text{nm}$. (b) Electromagnetic-field distribution of the resonant optical mode in PhC cavity.

Three pairs of mini air holes are placed inside the cavity with modified size and position as shown in Fig. 2(a). The first pair of air holes have reduced radii of $r_c = 0.78r$ and an outward position shift of $d_c = 0.2a$, which are 132.6nm and 103nm for our sensor. These two air holes enhance the light confinement in the lateral direction in the cavity [31]. The second pair of air holes is minimized holes without any location adjustment, hence $d_b = 0$. Their radii are shrunk to $r_b = 0.2r$ (34nm). The third pair has a slightly larger radii of $r_a = 0.28r$ (47.6nm) than the second pair, with the same positional shift of $d_a = 0.2a$ as the first pair.

Several resonant frequencies of such a cavity have been found within the bandgap. Their Q factor and intensity are shown in Fig. 3. For sensor applications, not only the quality factor is crucial to gain high sensitivity, but also the intensities of trapped photons at resonance are important. Among the calculated normalized resonant modes, those outside the region from 0.3 to 0.37 are undesirable modes for three reasons: 1) being close to the edge of the bandgap makes them susceptible to structural deviation, so their intensities are under the risk of decrease caused by band edge cutoff; 2) modes with frequencies higher than 0.37 have more

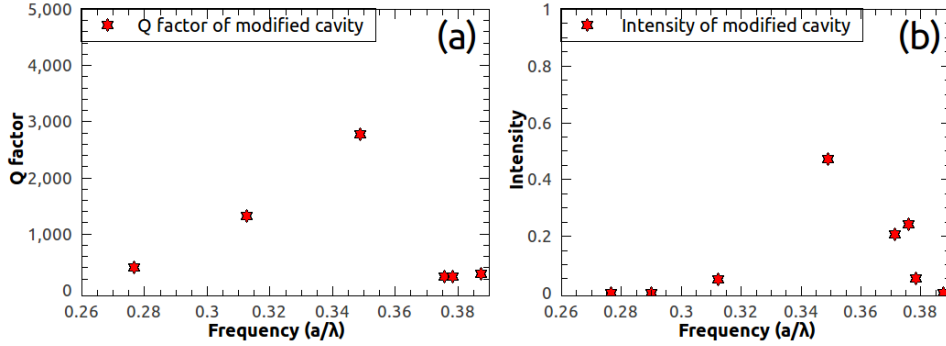


Fig. 3. Calculated Q factors (a) and intensities (b) of a modified L7 cavity with mini air holes.

than one neighboring resonant frequency, which may cause problems such as false data reading; 3) the intensities of those modes are quite low, at the levels from E-4 to E-7. Therefore, we focus our attention on the discrete resonance modes having both higher Q factor and higher intensity. In our case, these are normalized frequencies at 0.318 and 0.349.

The electromagnetic-field distributions of resonant modes are calculated by exciting narrower band Gaussian sources inside the cavity, centered at the frequencies of 0.318 and 0.349. As can be seen from Fig. 2(b), the field is continuous over the three pairs of mini air holes, with lobes overlapping with those mini air holes. This effect may make the cavity sensitive to refractive index changes due to enlarged overlapping area between light and matter inside these mini holes. At the frequency of 0.318, the calculated intrinsic Q factor and intensity are 1325 and 0.05. These values go much higher to 2773 and 0.5 at the frequency of 0.345. It should be noticed that although the Q factor and intensity presented here are calculated by exciting light sources inside the cavity, excitations from outside have similar effects. Photons coming from directly incident light or waveguide coupling are also trapped and stay inside the cavity during resonance.

Now we have optimized parameters of the cavity itself and parameters of additional mini air holes. Higher Q factor can be achieved by further modifying geometries of the cavity. However, we have chosen our sensor design as a compromise between an extremely high Q factor and strong light-matter interaction. To our knowledge, a Q factor of 1000 is sufficient to sense a refractive index change of $\Delta n = 5E-3$ at 1550nm with a sensitivity $S > 310$, according to these relations: $\Delta\lambda = \lambda/Q$, $\Delta n = \Delta\lambda/S = \lambda/(QS)$.

To illustrate the operating principle of the sensor and to quantitatively estimate its sensitivity, a series of three-dimensional FDTD simulations have been conducted. The simulation domain comprises the cavity itself with a lattice constant of 515nm, and a pair of single-mode photonic crystal waveguides as the light input/output ports. The holes of the photonic crystal are filled with air, water and ethanol of which refractive indices are set to be 1.0, 1.33 and 1.36 respectively.

Typical calculated output spectrum of the photonic crystal sensor is demonstrated in Fig. 4. The output spectra consist of multiple resonant peaks in the spectrum wherein each peak corresponds to one resonant frequency with specific electromagnetic-field distribution. Though the cavity sustains multiple modes, the resonant peaks are sufficiently separated. The existence of these multiple resonant peaks provides an extra confirmation of analyte identification, as all peaks will simultaneously sense the variance of refractive index. Shift in resonant frequency indicates a change in the RI of analytes. As can be seen, a change in the refractive index of $\Delta n = 3E-2$ between water and ethanol results in a spectral blue-shift of approximately 12.05 nm.

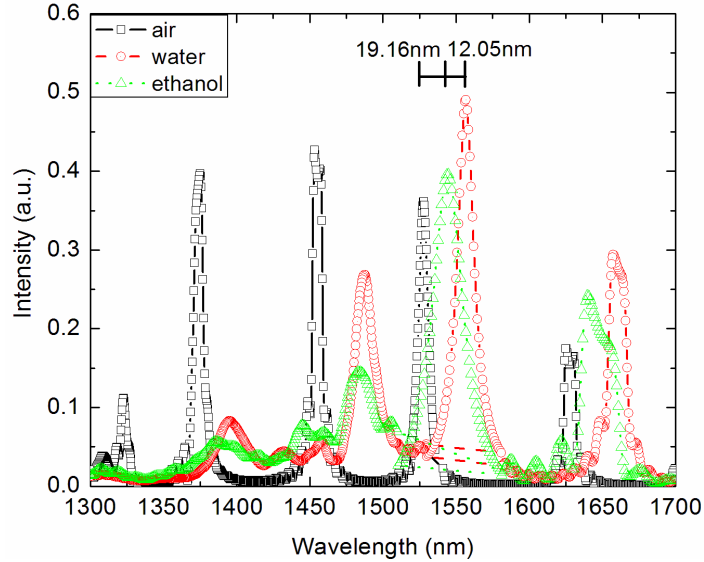


Fig. 4. Calculated transmission spectra of the sensor with air/water/ethanol infiltration. A change in refractive index of $\Delta n = 3E-2$ between water and ethanol results in a spectral blue-shift of 12.05 nm.

3. Fabrication

The flowchart of fabrication is shown in Fig. 5. The photonic crystal sensor was fabricated on silicon-on-insulator (SOI) wafer having a 220 nm-thick silicon membrane and a 2 μm -thick silicon dioxide box-layer. Fabrication of the device started from cleaning a 2 cm^2 SOI chip with nitric acid to remove any residual organics. ZEP520, a positive electron-beam resist, was spun on top of the SOI chip with an approximate thickness of 120 nm followed by a pre-baking at 175°C for 15 min to remove any residual solvent. The photonic crystal was patterned using a Leica EBPG 5000 + e-beam lithography system operating at 100 keV. The resist was developed with a microchem 1:3 MIBK:IPA solution for 30 s followed by a 10 s IPA rinse. Exposed areas of the SOI wafer were then etched using inductively coupled plasma (ICP) dry etching system with gas flow of 75 sccm SF₆ and 25 sccm O₂. Following the

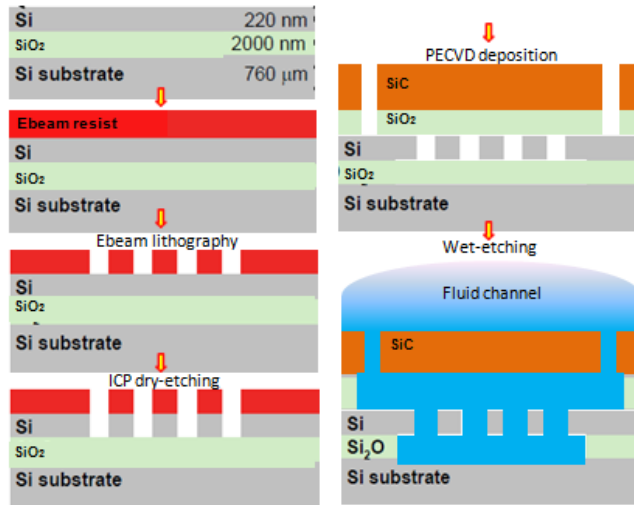


Fig. 5. Flowchart of sensor fabrication.

silicon etch, the remaining ZEP520 was dissolved in PRS3000 solution, and the chip was re-cleaned with Piranha solution (3:1 H₂SO₄:H₂O₂) to remove any surface contaminants.

For the reason of mechanical durability, the silicon dioxide box-layer was retained beneath the silicon membrane, except the sensor areas. In order to protect our sensor from physical damage, we deposited a 2μm-thick silicon dioxide layer on top of the photonic crystal and used another hard layer made of silicon carbide to cover the whole device. The thickness of silicon carbide layer was thicker than 3 μm in order to avoid sagging problem after wet etching. Fluidic accesses were opened by etching air holes through the silicon carbide layer, as shown in Fig. 6(b). These accesses fulfill two functions: firstly, pathways were created for the surrounding analytes to fill into the reaction sites. Secondly, undesired dirty particles were filtered out to keep the sensor clean. After the fluidic accesses had been opened, wet chemical etching of HF was applied to remove silicon dioxide both upon and beneath the sensor to create a suspended air-bridge photonic crystal as illustrated in Fig. 6(c). The etching time must be controlled properly based on multiple tests.

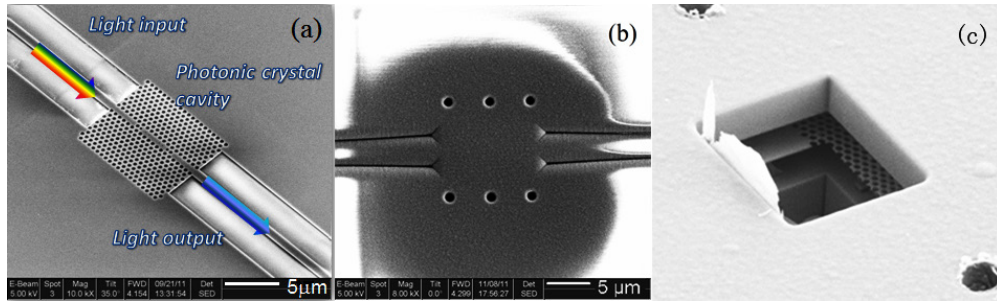


Fig. 6. (a) Scanning Electron Microscope image of sensor device after ICP etching. (b) Scanning Electron Microscope image of fluidic accesses on SiC layer. (c) An example of suspended photonic crystal under silicon carbide.

The utilization of micro fluidic channels provides spatial confinement of the analyte directly on the reaction site. For the reason of replication, a mold of fluidic channels was first created using a 4-inch pure silicon wafer. A 1μm-thick UV resist layer of AZ5214 was spun on top of the silicon followed by Near-UV lithography to write the patterns of fluidic channels. Pattern-transfer was done by reactive ion etching (RIE) to yield an etching depth of approximately 30μm. The PDMS elastomer was then poured onto the silicon mold and cured at 70°C for 6 hours to create flow channels. The elastomer was carefully peeled off to obtain the PDMS fluidic film. Once access holes have been punched through fluidic channels, the elastomer film can be chemically treated in order to seal the fluidic channels on top of the sensor chip. The PDMS film was oxidized with O₂ plasma to create a hydrophilic surface. Afterwards, a precise alignment of fluidic channels with sensors was insured by using an optical microscope setup during bonding process. Fluidic channels and sensor are aligned, quickly sealed as shown in Fig. 7, and post-baked at 170°C for 1 hour to increase the bonding strength between the fluidic film and the substrate. Finally, optical waveguides were exposed for measurement by hand-cleaving at the facets.

For our photonic crystal sensor, the resonant wavelength is near $\lambda = 1550$ nm. The lattice constant was therefore set to be $a = 515$ nm with the hole radius of $r = 170$ nm. The sensor consists of a central cavity, 9 rows of air holes on both sides along the Γ -M direction, and a pair of input and output photonic crystal waveguides. The photonic crystal waveguides are created by introducing a single line “defect” in the Γ -K direction with a length of $20a$. Coupling into and out of the PCW are accomplished by traditional tapered strip waveguides (Fig. 6(a)). The strip waveguides are 220 nm-tall and taper from 2.5 μm-wide at the chip edge to 890 nm-wide at the PCW interface, in order to minimize the mode mismatch between itself and the PCW.

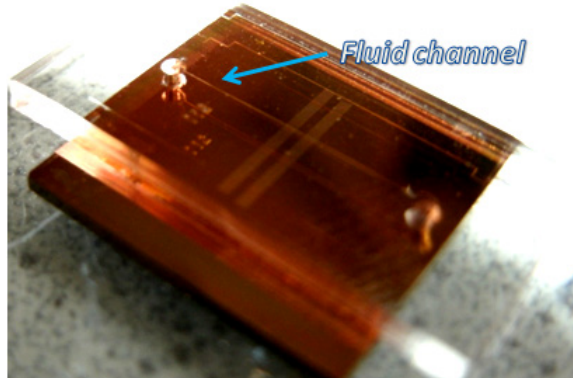


Fig. 7. Sealed elastomer-made fluidic channel on the sensor.

4. Experiment and analysis

A tunable laser source of Santec TSL-510 has a broadband power output from 3mW to 10mW, with wavelengths ranging from 1440nm to 1630nm. A polarization maintained lensed fiber is used to couple light from the laser to the input strip waveguide. TE polarization was selected before the fiber was mounted onto a three-axis optical stage at an extinction ratio of 100:1. The sample holder also has three-dimensional flexibilities in fine position adjustment. A group of objective lenses focused at the facet of the output strip waveguide. Output light is collected by a sensitive photon detector.

Syringes were used to inject analytes into the PDMS-made microfluidic channels. After each analyte was measured, the fluidic channels and the cavities were rinsed with acetone, isopropyl alcohol, and deionized water to remove any residual analyte. The entire chip was then baked on a hotplate at 120°C for 5 min to dry off the sensor. Transmission spectra of the sensors were confirmed every time as working under air-infiltrated condition before and after each analyte being injected into or flushed out of the fluidic channel.

Measured transmission spectra of our sensor are plotted in Fig. 8. As can be seen the photonic crystal cavity contributes sharp resonant peaks in the output spectra. Shifts of the resonant wavelengths are functions of refractive-index-variations of different analytes flowing through the channels. The black solid spectra, corresponding to air-infiltrated case, clearly show that the modified cavity design achieves a Q factor of 2600. The red and green spectra were obtained after the fluidic channels were infiltrated with water and ethanol respectively. Their refractive indices are 1.332 and 1.359. We observe very good matches between experimental data and theoretical simulations. In the presence of increased refractive indices, the resonant wavelength shifts are 22.28 nm for air/water infiltration and 12.65 nm for water/ethanol infiltration in experiments, while the simulated wavelength shifts were 19.16 nm and 12.05 nm for the same index changes.

We calculate the sensitivity of our sensor which is defined as the wavelength shift per refractive index unit (RIU). A slight index difference of 2.7E-2 results in a wavelength shift of 12.65nm. The device shows a sensitivity of 460 nm RIU^{-1} . Comparing the sensitivity of our device with L3 cavities, we can see an advantage in detection sensitivity. Under the same refractive index variation of 2.7E-2, L3 cavities with typical sensitivities about 100nm RIU^{-1} achieve a wavelength shift of only about 2.7nm. Obviously, our device provides a much clearer view of wavelength shift in transmission spectra.

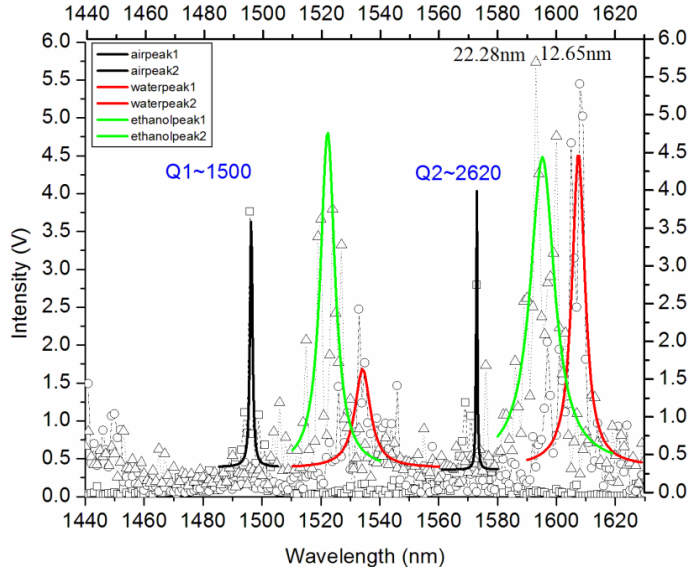


Fig. 8. Experimental transmission spectra of the sensor with air/water/ethanol infiltration. The red and green spectra were obtained after infilling channels with water and ethanol. A change in refractive index of $\Delta n = 2.7E-2$ between water and ethanol results in a spectral blue-shift of 12.65 nm.

5. Conclusions

We have demonstrated a two dimensional photonic crystal cavity as a sensitive optical sensor. Different from typical L3 cavity, this new structure consists of an optimized L7 cavity and three pairs of mini inside air holes. This design provides more than one resonant peak in transmission spectra which enable simultaneous identifications of the analytes. A protection layer made of silicon carbide was deposited on top of the sensors for mechanical durability. By sensing the refractive index change of the environmental solutions, a clear shift of resonant wavelength can be observed. A slight index difference of $2.7E-2$ results in a wavelength shift of 12.65 nm, which reflects a sensitivity of 460 nm per unit change in refractive index. The development of nano sensor devices is of great importance to environmental monitoring and detection. Our future plan is to optimize the Q factor of the sensor devices with fluidic infiltration to further improve the sensitivity, to increase signal-to-noise ratio to achieve higher resolution in detection, and to introduce cavity-array to fulfill the function of fingerprinting.

Acknowledgments

This work is supported by the project of FOM IPP IPOG-II: Nano Photonic Sensors (NPS). The authors would like to thank Stephen J. Picken from department of chemical Engineering of TU Delft in liquid index measurement and Shou-En Zhu from department of Precision and Microsystems Engineering of TU Delft for the help in elastomeric channel fabrication. Many appreciations also are given to our colleagues in “Photonic devices” group.